Endothelium-Derived Hydrogen Peroxide Accounts for the Enhancing Effect of an Angiotensin-Converting Enzyme Inhibitor on Endothelium-Derived Hyperpolarizing Factor–Mediated Responses in Mice

Takako Fujiki, Hiroaki Shimokawa, Keiko Morikawa, Hiroshi Kubota, Makoto Hatanaka, M.A. Hassan Talukder, Tetsuya Matoba, Akira Takeshita, Kenji Sunagawa

Background—We have recently identified that endothelium-derived hydrogen peroxide (H_2O_2) is an endothelium-derived hyperpolarizing factor (EDHF) in animals and humans, for which endothelial nitric oxide synthase (eNOS) is an important source. Angiotensin-converting enzyme (ACE) inhibitors are known to enhance EDHF-mediated responses. In this study, we examined whether endothelium-derived H_2O_2 accounts for the enhancing effect of an ACE inhibitor on EDHF-mediated responses and, if so, what mechanism is involved.

Methods and Results—Control and $eNOS^{-/-}$ mice were maintained with or without temocapril (10 mg/kg per day orally) for 4 weeks, and isometric tensions and membrane potentials of mesenteric arteries were recorded. In control mice, temocapril treatment significantly enhanced EDHF-mediated relaxations and hyperpolarizations to acetylcholine (n=8 each). Catalase, a specific scavenger of H_2O_2, abolished the beneficial effects of temocapril, although it did not affect endothelium-independent relaxations to sodium nitroprusside or NS1619, a direct opener of K_{Ca} channels (n=6 each). Western blot analysis demonstrated that the temocapril treatment significantly upregulated the expression of eNOS. By contrast, this enhancing effect of temocapril was absent in $eNOS^{-/-}$ mice (n=6).

Conclusions—These results indicate that endothelium-derived H_2O_2 accounts for the enhancing effect of temocapril on EDHF-mediated responses caused in part by eNOS upregulation, further supporting our H_2O_2 theory. (***Arterioscler Thromb Vasc Biol.* 2005;25:766-771.**)

Key Words: angiotensin-converting enzyme inhibitors ■ endothelium-derived factors ■ nitric oxide synthase ■ vasodilation

The endothelium plays an important role in maintaining vascular homeostasis by synthesizing and releasing several vasodilating factors, including prostacyclin, nitric oxide (NO), and endothelium-derived hyperpolarizing factor (EDHF).[1,2] It is widely accepted that EDHF plays an important role, especially in microvesseles.[3,4] There are several candidates for EDHF, including epoxyeicosatrienoic acids, gap junctions, K^+ ions,[5] and, as we have recently identified, hydrogen peroxide (H_2O_2).[4] H_2O_2 induces vascular relaxation and hyperpolarization.[6–9] We and others have subsequently identified that H_2O_2 is an EDHF in human mesenteric arteries[10] and porcine,[11] canine,[12] and human[13] coronary arteries. Furthermore, we have recently demonstrated that endothelial Cu/Zn-superoxide dismutase (SOD) plays a pivotal role to produce H_2O_2 as an "EDHF synthase" in mice.[14]

Angiotensin-converting enzyme (ACE) inhibitors are known to improve endothelial dysfunction in diabetes mellitus,[15] aging,[16] and patients with atherogenic risk factors.[17] ACE inhibitors are also known to enhance EDHF-mediated endothelium-dependent relaxation even in normal arteries.[18–20] However, the nature of EDHF involved in the beneficial effects of ACE inhibitors remains to be elucidated. In this study, we thus examined whether endothelium-derived H_2O_2 accounts for the enhancing effect of an ACE inhibitor on EDHF-mediated responses and, if so, what mechanism is involved to obtain further supporting evidence for our H_2O_2 theory.

Materials and Methods

This study was reviewed by the Committee of Ethics on Animal Experiments of Kyushu University and was performed according to the Guidelines for Animal Experiments of Kyushu University and of the Japanese Government.

Original received August 17, 2004; final version accepted January 26, 2005.

From the Department of Cardiovascular Medicine (T.F., H.S., K.M., H.K., M.H., M.A.T., T.M., A.T., K.S.), Kyushu University Graduate School of Medical Sciences, and the Kyushu University COE Program on Lifestyle-related Diseases (H.S.), Fukuoka, Japan.

Correspondence to Hiroaki Shimokawa, MD, PhD, Department of Cardiovascular Medicine, Kyushu University Graduate School of Medical Sciences, 3-1-1, Maidashi, Higashi-ku, Fukuoka 812-8582, Japan. E-mail shimo@cardiol.med.kyushu-u.ac.jp

Arterioscler Thromb Vasc Biol. **is available at http://www.atvbaha.org** **DOI: 10.1161/01.ATV.0000158498.19027.75**

Animal Preparation and Vessel Isolation

A total of 98 female C57BL/6N mice, obtained from a colony at Kyushu University were used. Female mice were used because of their availability in our institute. They were treated with oral administration of vehicle, temocapril (10 mg/kg per day) or hydralazine (20 mg/kg per day) for 4 weeks, from 12 to 16 weeks of age, in their drinking water. At the end of each treatment, body weight and systolic blood pressure were measured. Systolic blood pressure was measured by tail-cuff method under conscious conditions.[4,14] Then, the animals were anesthetized with pentobarbital (50 mg/kg intraperitoneal) and euthanized. The mesenteric arteries were carefully isolated and were cut into 1-mm and 1.5-mm rings for the measurements of both isometric tensions and membrane potentials.[4,14] To examine endothelium-independent responses, some arterial rings were stripped of the endothelium by gently rubbing. Twelve male endothelial nitric oxide synthase-deficient ($eNOS^{-/-}$) mice with the same age,[4] were also treated with oral administration of either vehicle or temocapril (10 mg/kg per day) for 4 weeks and used for Western blot analysis and isometric tension recordings.

Organ Chamber Experiments

Experiments were performed in 37°C Krebs solution bubbled with 95% O_2 and 5% CO_2. Arterial rings were mounted and isometric tension was measured by a force transducer (Nihon Kohden Co). Rings were precontracted with prostaglandin $F_{2\alpha}$ or KCl. The extent of precontraction was adjusted to ≈50% to 70% of the contractions induced by 62 mmol/L KCl.[4,14] Endothelium-dependent relaxations to acetycholine (ACh) and endothelium-independent relaxation to sodium-nitroprusside (SNP) or NS-1619, an opener of calcium-activated K channels (K_{Ca}), were examined.[3,4,21] The contribution of vasodilator prostaglandins, NO, and EDHF to ACh-induced endothelium-dependent relaxation was determined by the inhibitory effects of indomethacin (10 μmol/L), N^{ω}-nitro-L-arginine (L-NNA) (100 μmol/L), and KCl (30 to 50 mmol/L), respectively, by using area under the relaxation curves.[3,4,14,21] We confirmed that coincubation of carboxy-PTIO (300 μmol/L), a scavenger of NO, with indomethacin and L-NNA did not further inhibit NO-mediated relaxation, indicating that the concentration of L-NNA was sufficient to completely inhibit NO-mediated relaxation (data not shown). To examine the involvement of endothelium-derived H_2O_2 in the EDHF-mediated responses, the inhibitory effect of catalase, a specific scavenger of H_2O_2, was examined.[4,10–12,14] The effect of inactivated catalase by aminotriazole (50 mmol/L) was also examined to examine the specificity of catalase.[4,10–12]

Electrophysiological Experiments

The rings of small mesenteric arteries were placed in experimental chambers perfused with 37°C Krebs solution containing indomethacin (10 μmol/L) and L-NNA (100 μmol/L) bubbled with 95% O_2 and 5% CO_2. A fine glass capillary microelectrode was impaled into the smooth muscle from the adventitial side.[4,14] Changes in membrane potentials produced by ACh were continuously recorded.[4,14]

Measurements of Serum Concentrations of Temocaprilat and Estradiol

Blood samples were collected for measurements of serum concentrations of temocaprilat, an active form of temocapril, with an inhibitor-binding assay using high-performance liquid chromatography[22,23] and those of estradiol by radioimmunoassay. We centrifuged the blood samples for 10 minutes at 4°C and stored at −20°C until the measurements.

Western Blot Analysis

Western blot analysis for eNOS and Cu/Zn-SOD protein was performed using an antibody that specifically recognizes them.[4,14] The same amount of extracted protein from whole tissue of mesenteric arteries was loaded for SDS-PAGE/immunoblot analysis. Each band was normalized by corresponding value of β-actin as an internal control.[24]

SOD Activity

Cu/Zn-SOD activity of mesenteric arteries was measured by nitroblue tetrazolium method, as previously described.[14,25]

Catalase Activity

Catalase activity of mesenteric arteries was examined by automated assay based on the peroxidatic activity of the enzyme, as previously described.[14,26]

Glutathione Peroxidase Activity

Glutathione peroxidase activity of mesenteric arteries was determined by oxidation of NADPH in the presence of glutathione reductase, as previously described.[14]

Drugs

ACh, indomethacin, L-NNA, SNP, NS1619, hydralazine hydrochloride, catalase, and aminotriazole were purchased from Sigma Chemical Co (St. Louis, Mo). Temocapril was a gift from Sankyo Pharmaceutical Co (Tokyo, Japan).

Statistical Analysis

Results are expressed as mean±SEM. Throughout the text, n represents the number of animals tested. Dose–response curves were analyzed by 2-way ANOVA followed by Bonferroni post-hoc test for multiple comparisons. Other values were analyzed by unpaired Student t test or 1-way ANOVA. $P<0.05$ was considered to be statistically significant.

Results

Body Weight and Systolic Blood Pressure

After 4 weeks of maintenance, there was no significant difference in body weight (grams) among the control, temocapril, and hydralazine groups (22.2±0.5, 22.6±1.3, and 22.6±1.4, respectively). Systolic blood pressure (mm Hg) was significantly decreased in the temocapril group compared with the control group (92±3 versus 116±3; $P<0.001$). In the hydralazie group, systolic blood pressure was decreased to the same extent in the temocapril groups (93±3; $P<0.001$ versus control group).

Serum Concentrations of Temocaprilat and Estradiol

Serum concentrations of temocaplilat were detected only in the temocapril group (116±22.8 ng/mL, the detection level was 2 ng/mL). Serum concentrations of estradiol (pg/mL) were comparable among the control, temocapril, and hydralazine groups (12.8±0.7, 13.7±1.7, 12.9±0.8, respectively).

Endothelium-Dependent Relaxation

In the control group, endothelium-dependent relaxations to ACh of mesenteric arteries were sensitive to L-NNA (in the presence of indomethacin) and to KCl (in the presence of indomethacin and L-NNA), indicating an important role of NO and EDHF, respectively (Figure 1A and 1D). In the temocapril group, EDHF-mediated relaxations to ACh (in the presence of indomethacin and L-NNA) were significantly enhanced compared with the control group (Figure 1B and 1D). By contrast, the treatment with hydralazine did not enhance the EDHF-mediated relaxations (Figure 1C and 1D). The contribution of vasodilator prostaglandins was insignificant in all the groups (Figure 1).

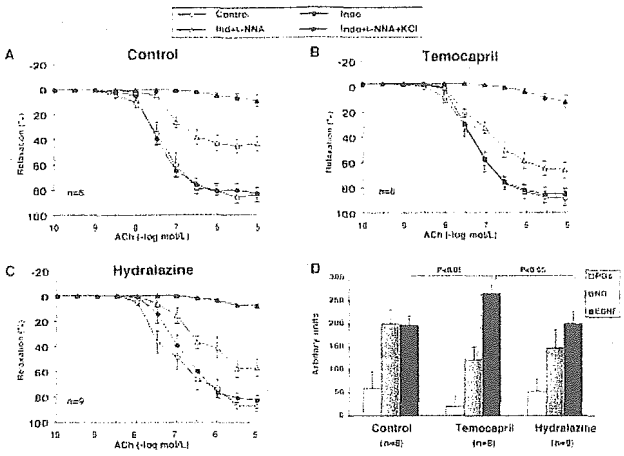

Figure 1. Enhancing effect of temocapril on EDHF-mediated relaxation of mouse mesenteric arteries. Endothelium-dependent relaxation to ACh in the control (A), temocapril (B), and hydralazine (C) groups and the relative contribution of vasodilator prostaglandins, NO, and EDHF to the ACh-induced relaxations in the 3 groups (D). EDHF-mediated relaxations to ACh (in the presence of indomethacin and L-NNA) were enhanced in the temocapril group but not in the hydralazine group. Results are expressed as means±SEM.

Catalase largely inhibited the EDHF-mediated relaxation in the control and the temocapril groups, but when inactivated by aminotriazole, catalase lost its inhibitory effect, indicating a substantial involvement of H_2O_2 in the enhancing effect of temocapril on the EDHF-mediated relaxations (Figure 2).

Endothelium-Dependent Hyperpolarization

Resting membrane potentials were significantly more negative in the temocapril group than in the control group, and the ACh-induced hyperpolarization was significantly larger in the temocapril group (Figure 3A and 3B). The enhancing effect of temocapril on the ACh-induced hyperpolarization was markedly inhibited by catalase (Figure 3B). There was no significant difference in the resting potential or the ACh-induced hyperpolrization between the control and the hydralazine groups (Figure 3A and 3B).

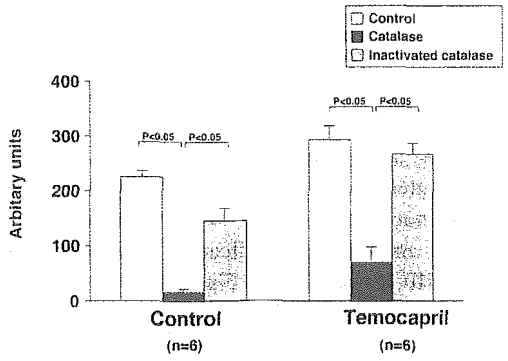

Figure 2. Involvement of H_2O_2 in the enhancing effect of temocapril on the EDHF-mediated relaxations. Catalase (6250 U/mL) markedly inhibited the EDHF-mediated relaxation in both the control and temocapril groups, whereas it lost its inhibitory effect when inactivated by aminotriazole (50 mmol/L). Results are expressed as means±SEM.

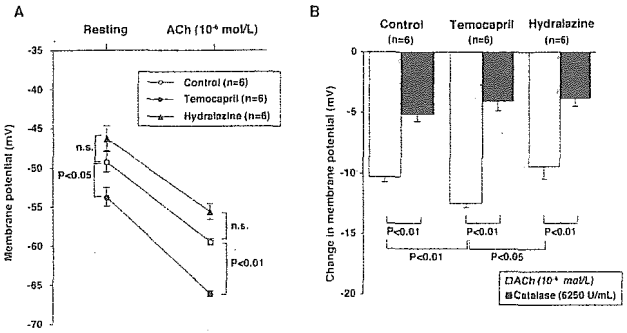

Figure 3. Enhancing effect of temocapril on the EDHF-mediated hyperpolarizations under resting conditions (A) and in response to ACh (B). Results are expressed as means±SEM.

Endothelium-Independent Relaxation

There was no significant difference in the endothelium-independent relaxations to SNP or NS1619 between the control and the temocapril groups (Figure I, available online at http://atvb.ahajournals.org). Furthermore, those relaxations to SNP or NS1619 were unaltered in the presence of indomethacin, L-NNA, or catalase (data not shown).

Protein Expression of eNOS and Cu/Zn-SOD

The expression of eNOS protein in the mesenteric arteries was significantly higher in the temocapril group compared with the control group (Figure 4A), whereas the expression of Cu/Zn-SOD protein was comparable between the 2 groups (Figure 4B).

Enzyme Activities

The vascular activity of Cu/Zn-SOD, catalase, or glutathione peroxidase was comparable between the control and the temocapril groups (Figure II, available online at http://atvb.ahajournals.org).

Endothelium-Dependent Relaxations in eNOS$^{-/-}$ Mice

After 4 weeks of maintenance, there was no significant difference in body weight (grams) between the control (untreated) and the temocapril-treated eNOS$^{-/-}$ mice (25.7±1.2 and 22.3±0.9, respectively). The treatment with

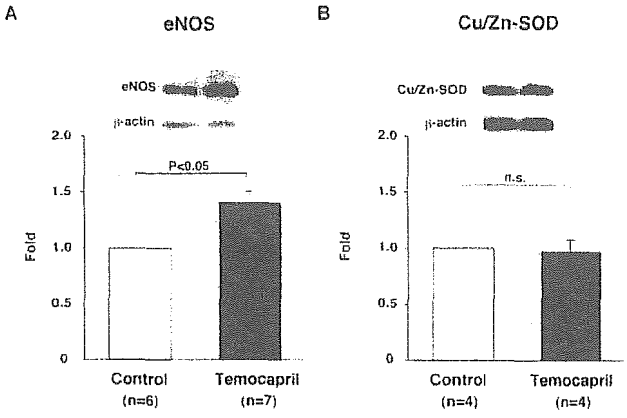

Figure 4. Expression of eNOS (A) and Cu/Zn-SOD (B) protein. The temocapril treatment significantly enhanced the former but not the latter. Results are expressed as means±SEM.

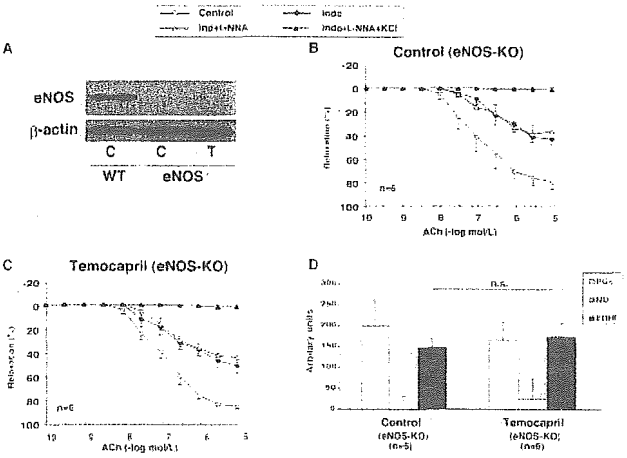

Figure 5. Effect of temocapril on EDHF-mediated relaxations of mesenteric arteries from $eNOS^{-/-}$ mouse. A, Expression of eNOS was absent in the $eNOS^{-/-}$ mice. B, There was a marked compensatory involvement of vasodilator prostaglandins, absence of NO activity, and a residual activity of EDHF, respectively, in the untreated $eNOS^{-/-}$ mice. C, There was no effect of temocapril on the EDHF-mediated relaxations to ACh of mesenteric arteries from $eNOS^{-/-}$ mice. D, The relative contribution of vasodilator prostaglandins, NO, and EDHF to the ACh-induced relaxations in the control (untreated) and temocapril-treated $eNOS^{-/-}$ mice.

temocapril significantly decreased systolic blood pressure (131±5 versus 85±5 mm Hg; $P<0.001$). In both control and temocapril-treated $eNOS^{-/-}$ mice, protein expression of eNOS was undetectable (Figure 5A). In the control $eNOS^{-/-}$ mice, endothelium-dependent relaxations to ACh were markedly sensitive to indomethacin but resistant to L-NNA (in the presence of indomethacin), and partially sensitive to KCl (in the presence of indomethacin and L-NNA), indicating a marked compensatory role of vasodilator prostaglandins with residual EDHF activity (Figure 5B and 5D). In the temocapril-treated $eNOS^{-/-}$ mice, EDHF-mediated relaxations to ACh were unaltered, a contrast finding with that in C57BL/6N mice (Figure 5C and 5D).

Discussion

The major findings of the present study were as follows: (1) the long-term treatment with temocapril significantly enhanced EDHF-mediated relaxations and hyperpolarizations to ACh of mouse mesenteric arteries; (2) the enhancing effects of temocapril on the EDHF-mediated responses were mediated primarily by H_2O_2; (3) the enhanced expression of eNOS may be involved in the effect of temocapril, whereas vascular enzyme activities, including those of Cu/Zn-SOD, catalase, or glutathione peroxidase, were unaltered by the temocapril treatment; and (4) the enhancing effects of temocapril on the EDHF-mediated responses were not observed in $eNOS^{-/-}$ mice. These results demonstrate that endothelium-derived H_2O_2 accounts for the enhancing effect of an ACE inhibitor on the EDHF-mediated responses, further confirming our EDHF/H_2O_2 theory.[4,10–12,14]

Enhancing Effect of Temocapril on EDHF-Mediated Responses in Normal Mice

In the temocapril group, EDHF-mediated relaxations were significantly enhanced as compared with the control group. This effect of temocapril was not caused by its blood pressure-lowering effect because the same extent of reduction in blood pressure by hydralazine did not enhance the EDHF-mediated responses. This finding is consistent with our previous study in which long-term treatment with an ACE inhibitor, but not that with hydralazine, ameliorated aging-related endothelial dysfunction in rats.[16]

Estrogen is known to enhance EDHF-mediated relaxations of rat mesenteric arteries.[27] Because we used female mice in the present study because of the availability of animals, we measured serum concentrations of estradiol and confirmed that the concentrations were comparable among the control, temocapril, and hydralazine groups. Therefore, it is unlikely that the enhanced EDHF-mediated relaxation in the temocapril group was caused by menstrual cycle of the animals or to the increased concentration of estradiol by temocapril. Because in the temocapril group catalase markedly inhibited the enhanced EDHF-mediated responses and inactivated catalase lost its inhibitory effect, increased endothelial production of H_2O_2 appears to play a primary role in the enhancing effects of temocapril on the EDHF-mediated responses.

Possible Mechanism Involved in the Enhancing Effect of an ACE Inhibitor on EDHF-Mediated Responses

Long-term treatment with an ACE inhibitor temocapril is known to improve endothelial dysfunction in diabetes mellitus,[15] aging,[16] and hypertension.[17] It has been reported that the mechanisms of the beneficial effects of ACE inhibitors include an inhibition of bradykinin degradation,[28] suppression of oxidative stress,[29,30] and enhancement of eNOS activity.[31,32] ACE inhibitors upregulate eNOS mRNA expression that may result from the inhibition of kininase II that catalyzes the degradation of bradykinin.[31] In the present study, the expression of eNOS protein in the temocapril group was significantly enhanced ≈1.4-fold as compared with the control group. This is consistent with the previous study in which eNOS protein expression was significantly enhanced in nondiabetic rats with an ACE inhibitor.[33]

ACE inhibitors are known to increase eNOS expression and its activity via increasing bradykinin content,[34] and a bradykinin B_2 receptor antagonist, HOE-140, inhibits the effect of ACE inhibitors even in normal animals.[35] It is reported that the vascular effects of temocapril are also mediated through the bradykinin pathway.[36] In the present study, because eNOS expression was increased ≈1.4-fold in the temocapril group, the bradykinin pathway may play an important role in the upregulation of eNOS induced by the treatment. The upregulated eNOS may enhance EDHF-mediated relaxation, because we have previously demonstrated that eNOS plays an important role in producing H_2O_2 as an EDHF.[4]

eNOS consists of 2 domains, oxygenase and reductase domains, and the coupling of the 2 domains is not so tight as compared with the other 2 isoforms, nNOS and iNOS.[37] Thus unlike nNOS or iNOS, eNOS produces superoxide anions from reductase domain even under physiological conditions, and this process is resistant to L-arginine analogues.[37] eNOS produces superoxide anions from the oxygenase domain only

when the uncoupling of the 2 domains is accelerated by tetrahydrobiopterin or L-arginine deficiency, the process of which is sensitive to L-arginine analogues.[37–39] Because we examined endothelial function under physiological conditions with and without an ACE inhibitor treatment, it is not surprising that endothelial production of superoxide is resistant to L-arginine analogues. Thus, eNOS could serve as a source of H_2O_2 even in the presence of L-NNA.[40,41] In our previous study, we confirmed that endothelial production of H_2O_2 was unaffected by indomethacin or L-NNA.[4] Thus, H_2O_2 derived from eNOS can be synthesized and act as an EDHF in the presence of indomethacin and L-NNA.[4] It is thus conceivable that H_2O_2 released from upregulated eNOS by an ACE inhibitor is able to cause vasodilatation and hyperpolarization.

Heat shock protein 90 (hsp90), one of the eNOS-associated proteins, is known to be coupled with eNOS for NO generation.[42] Because inhibition of hsp90 is sufficient to uncouple eNOS activity and lead to increased superoxide generation,[43] it remains to be examined whether this mechanism is involved in the present finding with temocapril.

To confirm the involvement of eNOS upregulation in the effect of an ACE inhibitor, we further examined the effect of temocapril in $eNOS^{-/-}$ mice. In those mice, there was no eNOS protein expression in control or temocapil-treated animals. Importantly, temocapril failed to enhance EDHF-mediated relaxations in those mice, indicating that the enhancing effect of temocapril on EDHF-mediated responses is mediated, at least in part, by eNOS upregulation by the ACE inhibitor.

Recently, we have demonstrated that endothelial Cu/Zn-SOD plays an important role in producing H_2O_2 as an EDHF synthase in mouse mesenteric arteries.[14] In the present study, we found no significant difference in the expression of Cu/Zn-SOD or its activity, as well as other vascular enzyme activities. H_2O_2 might be produced not only by SOD but also by spontaneous conversion from superoxide,[9] and this point remains to be examined in future studies.

ACE inhibitors are known to have radical scavenging effects. Captopril, for example, has the protective action on endothelium-dependent relaxation like SOD, by scavenging basally released oxygen-derived free radicals.[44] In general, ACE inhibitors with sulfhydryl group (SH) are known to have a scavenging effect of oxygen-derived free radicals.[44] However, it is also possible that temocapril, a non-SH–containing ACE inhibitor, has a radical scavenging effect because several studies have demonstrated that the presence of SH group is not the only determinant for the antioxidant properties of ACE inhibitors.[45,46] Thus, the results with temocapril in the present study might be explained in part by the direct effect of the ACE inhibitor in scavenging basally released oxygen-derived free radicals.

Limitations of the Study

Several limitations should be mentioned for the present study. First, we only examined the long-term effect of an ACE inhibitor on EDHF-mediated responses in normal and $eNOS^{-/-}$ mice. Thus, it remains to be examined in future studies whether endothelium-derived H_2O_2 also is involved in the effects of ACE inhibitors on the reduced EDHF-mediated responses under various pathological conditions. Second, in the present study, we did not directly demonstrate the enhanced endothelial production of H_2O_2 in the temocapril group. We have recently succeeded in measuring endothelial production of endothelium-derived H_2O_2 with electron spin resonance method in porcine coronary arteries,[11] but not in mouse mesenteric arteries yet, because of the limited availability of endothelial cells. This point also remains to be addressed in a future study.

Clinical Implications

EDHF plays an important role in human arteries to maintain endothelium-dependent relaxations,[21,47] especially in patients with multiple risk factors.[21] ACE inhibitors are now widely used for the treatment of patients with hypertension,[48] acute and chronic heart failure,[49] myocardial infarction,[50] and diabetes mellitus.[51] ACE inhibitors also prevent endothelial dysfunction in patients with coronary artery disease.[52] In the present study, the serum concentration of temocaprilat in mice was equivalent to that of elderly patients receiving daily dose of temocapril.[22] We and others have demonstrated that endothelium-derived H_2O_2 is an EDHF in human mesenteric[10] and coronary arteries.[13] Thus, our present findings may contribute to our better understanding of the beneficial effects of ACE inhibitors on EDHF/H_2O_2-mediated responses in the clinical setting.

Acknowledgments

This work was supported in part by the grant for the 21st Century COE Program and grants-in-aid (13307024, 13557068, 15256003, 16209027) from the Japanese Ministry of Education, Science, Sports, and Culture, Tokyo, Japan. We thank E. Gunshima for excellent technical assistance in this study.

References

1. Mombouli JV, Vanhoutte PM. Endothelium-derived hyperpolarizing factor(s): updating the unknown. *Trends Pharmacol Sci.* 1997;18:252–256.
2. Shimokawa H. Primary endothelial dysfunction: atherosclerosis. *J Mol Cell Cardiol.* 1999;31:23–37.
3. Shimokawa H, Yasutake H, Fujii K, Owada MK, Nakaike R, Fukumoto Y, Takayanagi T, Nagao T, Egashira K, Fujishima M, Takeshita A. The importance of the hyperpolarizing mechanism increases as the vessel size decreases in endothelium-dependent relaxations in rat mesenteric circulation. *J Cardiovasc Pharmacol.* 1996;28:703–711.
4. Matoba T, Shimokawa H, Nakashima M, Hirakawa Y, Mukai Y, Hirano K, Kanaide H, Takeshita A. Hydrogen peroxide is an endothelium-derived hyperpolarizing factor in mice. *J Clin Invest.* 2000;106:1521–1530.
5. Busse R, Edwards G, Feletou M, Fleming I, Vanhoutte PM, Weston AH. EDHF: bringing the concepts together. *Trends Pharmacol Sci.* 2002;23:374–380.
6. Beny JL, von der Weid PY. Hydrogen peroxide: an endogenous smooth muscle cell hyperpolarizing factor. *Biochem Biophys Res Commun.* 1991;176:378–384.
7. Rubanyi GM, Vanhoutte PM. Oxygen-derived free radicals, endothelium, and responsiveness of vascular smooth muscle. *Am J Physiol.* 1986;250:H815–H821.
8. Thengchaisri N, Kuo L. Hydrogen peroxide induces endothelium-dependent and -independent coronary arteriolar dilation: role of cyclooxygenase and potassium channels. *Am J Physiol Heart Circ Physiol.* 2003;285:H2255–H2263.
9. Sato A, Sakuma I, Gutterman DD. Mechanism of dilation to reactive oxygen species in human coronary arterioles. *Am J Physiol Heart Circ Physiol.* 2003;285:H2345–H2354.

10. Matoba T, Shimokawa H, Kubota H, Morikawa K, Fujiki T, Kunihiro I, Mukai Y, Hirakawa Y, Takeshita A. Hydrogen peroxide is an endothelium-derived hyperpolarizing factor in human mesenteric arteries. *Biochem Biophys Res Commun.* 2002;290:909–913.
11. Matoba T, Shimokawa H, Morikawa K, Kubota H, Kunihiro I, Urakami-Harasawa L, Mukai Y, Hirakawa Y, Akaike T, Takeshita A. Electron spin resonance detection of hydrogen peroxide as an endothelium-derived hyperpolarizing factor in porcine coronary microvessels. *Arterioscler Thromb Vasc Biol.* 2003;23:1224–1230.
12. Yada T, Shimokawa H, Hiramatsu O, Kajita T, Shigeto F, Goto M, Ogasawara Y, Kajiya F. Hydrogen peroxide, an endogenous endothelium-derived hyperpolarizing factor, plays an important role in coronary autoregulation in vivo. *Circulation.* 2003;107:1040–1045.
13. Miura H, Bosnjak JJ, Ning G, Saito T, Miura M, Gutterman DD. Role for hydrogen peroxide in flow-induced dilation of human coronary arterioles. *Circ Res.* 2003;92:e31–e40.
14. Morikawa K, Shimokawa H, Matoba T, Kubota H, Akaike T, Talukder MA, Hatanaka M, Fujiki T, Maeda H, Takahashi S, Takeshita A. Pivotal role of Cu,Zn-superoxide dismutase in endothelium-dependent hyperpolarization. *J Clin Invest.* 2003;112:1871–1879.
15. Pieper GM, Siebeneich W. Temocapril, an angiotensin converting enzyme inhibitor, protects against diabetes-induced endothelial dysfunction. *Eur J Pharmacol.* 2000;403:129–132.
16. Mukai Y, Shimokawa H, Higashi M, Morikawa K, Matoba T, Hiroki J, Kunihiro I, Talukder HM, Takeshita A. Inhibition of renin-angiotensin system ameliorates endothelial dysfunction associated with aging in rats. *Arterioscler Thromb Vasc Biol.* 2002;22:1445–1450.
17. Iwatsubo H, Nagano M, Sakai T, Kumamoto K, Morita R, Higaki J, Ogihara T, Hata T. Converting enzyme inhibitor improves forearm reactive hyperemia in essential hypertension. *Hypertension.* 1997;29:286–290.
18. Goto K, Fujii K, Onaka U, Abe I, Fujishima M. Renin-angiotensin system blockade improves endothelial dysfunction in hypertension. *Hypertension.* 2000;36:575–580.
19. Vanhoutte PM. Endothelium-dependent responses and inhibition of angiotensin-converting enzyme. *Clin Exp Pharmacol Physiol.* 1996;23:S23–S29.
20. Feletou M, Vanhoutte PM. EDHF: new therapeutic targets? *Pharmacol Res.* 2004;49:565–580.
21. Urakami-Harasawa L, Shimokawa H, Nakashima M, Egashira K, Takeshita A. Importance of endothelium-derived hyperpolarizing factor in human arteries. *J Clin Invest.* 1997;100:2793–2799.
22. Arakawa M, Sasaki M, Ohmori M, Harada K, Fujimura A. Pharmacokinetics and pharmacodynamics of temocapril during repeated dosing in elderly hypertensive patients. *Eur J Clin Pharmacol.* 2001;56:775–779.
23. Shioya H, Shimojo M, Kawahara Y. Determination in plasma of angiotensin-converting enzyme inhibitor by inhibitor-binding assay. *J Chromatogr.* 1991;568:309–314.
24. Abe K, Shimokawa H, Morikawa K, Uwatoku T, Oi K, Matsumoto Y, Hattori T, Nakashima Y, Kaibuchi K, Sueishi K, Takeshit A. Long-term treatment with a Rho-kinase inhibitor improves monocrotaline-induced fatal pulmonary hypertension in rats. *Circ Res.* 2004;94:385–393.
25. Beauchamp C, Fridovich I. Superoxide dismutase: improved assays and an assay applicable to acrylamide gels. *Anal Biochem.* 1971;44:276–287.
26. Wheeler CR, Salzman JA, Elsayed NM, Omaye ST, Korte DW, Jr. Automated assays for superoxide dismutase, catalase, glutathione peroxidase, and glutathione reductase activity. *Anal Biochem.* 1990;184:193–199.
27. Liu MY, Hattori Y, Fukao M, Sato A, Sakuma I, Kanno M. Alterations in EDHF-mediated hyperpolarization and relaxation in mesenteric arteries of female rats in long-term deficiency of oestrogen and during oestrus cycle. *Br J Pharmacol.* 2001;132:1035–1046.
28. Cachofeiro V, Sakakibara T, Nasjletti A. Kinins, nitric oxide, and the hypotensive effect of captopril and ramiprilat in hypertension. *Hypertension.* 1992;19:138–145.
29. Rajagopalan S, Harrison DG. Reversing endothelial dysfunction with ACE inhibitors. A new trend. *Circulation.* 1996;94:240–243.
30. de Cavanagh EM, Inserra F, Toblli J, Stella I, Fraga CG, Ferder L. Enalapril attenuates oxidative stress in diabetic rats. *Hypertension.* 2001;38:1130–1136.
31. De Gennaro Colonna V, Rossoni G, Rigamonti A, Bonomo S, Manfredi B, Berti F, Muller E. Enalapril and quinapril improve endothelial vasodilator function and aortic eNOS gene expression in L-NAME-treated rats. *Eur J Pharmacol.* 2002;450:61–66.
32. Gonzalez Bosc LV, Kurnjek ML, Muller A, Terragno NA, Basso N. Effect of chronic angiotensin II inhibition on the nitric oxide synthase in the normal rat during aging. *J Hypertens.* 2001;19:1403–1409.
33. Trauernicht AK, Sun H, Patel KP, Mayhan WG. Enalapril prevents impaired nitric oxide synthase-dependent dilatation of cerebral arterioles in diabetic rats. *Stroke.* 2003;34:2698–2703.
34. Cargnoni A, Comini L, Bernocchi P, Bachetti T, Ceconi C, Curello S, Ferrari R. Role of bradykinin and eNOS in the anti-ischaemic effect of trandolapril. *Br J Pharmacol.* 2001;133:145–153.
35. Bachetti T, Comini L, Pasini E, Cargnoni A, Curello S, Ferrari R. ACE-inhibition with quinapril modulates the nitric oxide pathway in normotensive rats. *J Mol Cell Cardiol.* 2001;33:395–403.
36. Shiuchi T, Cui TX, Wu L, Nakagami H, Takeda-Matsubara Y, Iwai M, Horiuchi M. ACE inhibitor improves insulin resistance in diabetic mouse via bradykinin and NO. *Hypertension.* 2002;40:329–334.
37. Stuehr D, Pou S, Rosen GM. Oxygen reduction by nitric-oxide synthases. *J Biol Chem.* 2001;276:14533–14536.
38. Landmesser U, Dikalov S, Price SR, McCann L, Fukai T, Holland SM, Mitch WE, Harrison DG. Oxidation of tetrahydrobiopterin leads to uncoupling of endothelial cell nitric oxide synthase in hypertension. *J Clin Invest.* 2003;111:1201–1209.
39. Xia Y, Tsai AL, Berka V, Zweier JL. Superoxide generation from endothelial nitric-oxide synthase. A Ca2+/calmodulin-dependent and tetrahydrobiopterin regulatory process. *J Biol Chem.* 1998;273:25804–25808.
40. Vasquez-Vivar J, Kalyanaraman B, Martasek P, Hogg N, Masters BS, Karoui H, Tordo P, Pritchard KA, Jr. Superoxide generation by endothelial nitric oxide synthase: the influence of cofactors. *Proc Natl Acad Sci U S A.* 1998;95:9220–9225.
41. Stroes E, Hijmering M, van Zandvoort M, Wever R, Rabelink TJ, van Faassen EE. Origin of superoxide production by endothelial nitric oxide synthase. *FEBS Lett.* 1998;438:161–164.
42. Fleming I, Busse R. Molecular mechanisms involved in the regulation of the endothelial nitric oxide synthase. *Am J Physiol Regul Integr Comp Physiol.* 2003;284:R1–R12.
43. Ou J, Ou Z, Ackerman AW, Oldham KT, Pritchard KA, Jr. Inhibition of heat shock protein 90 (hsp90) in proliferating endothelial cells uncouples endothelial nitric oxide synthase activity. *Free Radic Biol Med.* 2003;34:269–276.
44. Mittra S, Singh M. Possible mechanism of captopril induced endothelium-dependent relaxation in isolated rabbit aorta. *Mol Cell Biochem.* 1998;183:63–67.
45. Moroi M, Akatsuka N, Fukazawa M, Hara K, Ishikawa M, Aikawa J, Namiki A, Yamaguchi T. Endothelium-dependent relaxation by angiotensin-converting enzyme inhibitors in canine femoral arteries. *Am J Physiol.* 1994;266:H583–H589.
46. Fernandes AC, Filipe PM, Freitas JP, Manso CF. Different effects of thiol and nonthiol ace inhibitors on copper-induced lipid and protein oxidative modification. *Free Radic Biol Med.* 1996;20:507–514.
47. Inokuchi K, Hirooka Y, Shimokawa H, Sakai K, Kishi T, Ito K, Kimura Y, Takeshita A. Role of endothelium-derived hyperpolarizing factor in human forearm circulation. *Hypertension.* 2003;42:919–924.
48. Gavras H, Brunner HR. Role of angiotensin and its inhibition in hypertension, ischemic heart disease, and heart failure. *Hypertension.* 2001;37:342–345.
49. Talbert RL. Treatment of acute and chronic heart failure. *J Am Pharm Assoc (Washington DC).* 2003;43:S18–S19.
50. Salam AM. Clinical trials evaluating angiotensin-converting enzyme inhibitors and angiotensin receptor blockers in the setting of acute myocardial infarction. *Expert Opin Investig Drugs.* 2003;12:501–507.
51. Fonarow GC. The management of the diabetic patient with prior cardiovascular events. *Rev Cardiovasc Med.* 2003;4(Suppl 6):S38–S49.
52. Mancini GB, Henry GC, Macaya C, O'Neill BJ, Pucillo AL, Carere RG, Wargovich TJ, Mudra H, Luscher TF, Klibaner MI, Haber HE, Uprichard AC, Pepine CJ, Pitt B. Angiotensin-converting enzyme inhibition with quinapril improves endothelial vasomotor dysfunction in patients with coronary artery disease. The TREND (Trial on Reversing ENdothelial Dysfunction) Study. *Circulation.* 1996;94:258–265.

Available online at www.sciencedirect.com
SCIENCE DIRECT®
Comput. Methods Appl. Mech. Engrg. 194 (2005) 4027–4047
Computer methods in applied mechanics and engineering
www.elsevier.com/locate/cma

A robust preconditioner for fluid–structure interaction problems

T. Washio [a,b], T. Hisada [b,*], H. Watanabe [b], T.E. Tezduyar [c]

[a] *Japan Science and Technology Agency CREST, Japan*
[b] *Graduate School of Frontier Science, University of Tokyo, 7-3-1 Hongo, Bunkyo-ku, Tokyo 113-0033, Japan*
[c] *Mechanical Engineering, Rice University, MS 321, 6100 Main Street, Houston, TX 77005, USA*

Received 28 October 2003; received in revised form 7 September 2004; accepted 1 October 2004

Abstract

Two preconditioners are presented for equation systems of strongly coupled fluid–structure interaction computations where the structure is modeled by shell elements. These preconditioners fall into the general category of incomplete LU factorization. The two differ mainly in whether the coefficient matrix is factorized node by node or variable-by-variable. In the variable-wise preconditioner, a modified Schur complement system for pressure is solved approximately with a few iterations using a special preconditioner. The efficiencies of the two preconditioners are compared for different finite element formulations of the fluid mechanics part, including formulations with SUPG and PSPG stabilizations.

Keywords: Iterative linear solver; Fluid–structure interaction; Preconditioner; Krylov subspace

1. Introduction

This paper provides two preconditioners for strongly coupled fluid–structure interaction problems. The preconditioners are incorporated into Krylov subspace methods like GMRES [9] or FGMRES [10] to solve systems of linear equations arising from Newton–Raphson iterations for solving non-linear fluid–structure interaction problems. Both preconditioners are based on the incomplete LU (ILU) factorization of the coefficient matrix. The ILU factorization is the most commonly used preconditioning technique for a broad

* Corresponding author.
E-mail addresses: washio@sml.k-u.tokyo.ac.jp (T. Washio), hisada@mech.t.u-tokyo.ac.jp (T. Hisada), nabe@sml.k.t.u-tokyo.ac.jp (H. Watanabe), tezduyar@rice.edu (T.E. Tezduyar).

0045-7825/$ - see front matter
doi:10.1016/j.cma.2004.10.001

range of applications. For the large majority of preconditioners, some kind of diagonal dominance is required to realize good convergence. This is also true for ILU preconditioners. Therefore, standard ILU preconditioners often fail for so called saddle point problems that arise, for example, in finite element and finite volume discretizations of Stokes equations, equations of hyper-elasticity, and mixed finite element discretization of second-order problems. It is also true that positive-definiteness alone is not a sufficient condition for the success of the ILU preconditioner. For example, it is well-known that ILU preconditioners often fail for shell problems. Thus, direct methods like sparse LU factorization are commonly applied in this area.

Finite element discretizations of fluid–structure coupled problems [17] show the above mentioned difficulties both in the Navier–Stokes part and the shell part. Furthermore, we also have to deal with the interaction of the two parts in the linear system for the strong coupling approach. Thus, a standard ILU preconditioning, without any special treatment for addressing the above difficulties, will fail. In this paper, we try to construct efficient and robust ILU-type preconditioners by taking measures to address these problems. In developing these preconditioners, we order the unknowns and equations based on the variable (fluid velocity, fluid pressure, or shell structure), and treat each block in the matrix system differently based on the variables with which they are associated. Similar selective treatment approaches were proposed in [11,12] for fluid–particle interactions. We note that information regarding the unknown variable is not usually exploited in the standard ILU factorization approach, though the node set information is frequently used.

In Section 2, the linear system which arises in the strongly coupled fluid–structure formulation is given. In these problems, there are four kinds of variables: the velocity vector of the fluid independent of the structure (V_i^f), the pressure vector of the fluid (P), the velocity vector of the common part of the fluid and the structure (V_c), and the velocity vector of the structure independent of the fluid (V_i^s). In the present problem where the structure part is composed of shell elements, unknowns in V_c and V_i^s are on the same nodes, and therefore, we combine them into a single unknown labeled with V^s. Thus, the coefficient matrix can be displayed in either three-by-three or four-by-four block form, providing unknowns and associated linear equations are ordered by variable. In this paper, we will adopt the three-by-three block form where the whole space is composed of V_i^f, P and V^s. In Section 3, we introduce the basic ideas of preconditioned Krylov subspace iterative methods. In particular, we will show the advantage of using Krylov subspace methods compared to a classical iterative method. Some features of the ILU preconditioning techniques are also explained as background information in introducing our methods. In Section 4, details of the two approaches for the velocity–pressure interaction in the fluid part are introduced. In the first approach, we use a strategy similar to one proposed in [2,13] where the coupled system is preconditioned under the ordering: $V_i^f \rightarrow P$. With this strategy, the loss of the diagonal entries on the pressure vector space P can be avoided. In the second approach, we first replace the main diagonal block associated with the velocity vector by its ILU factorized matrix. Then, the block LU factorization is applied to the 2×2 block system composed of the velocity and pressure variables. In the block factorization, the Schur complement on the pressure vector space is not given explicitly since it results in a dense matrix. Instead, the Schur complement system on the pressure vector is approximately solved by a small number of GMRES iterations with an appropriate preconditioner. Such an approach is related to the observations made in [6,7]. In Section 5, the two approaches on the fluid part are extended to the total system of fluid–structure coupling. The first approach is again a standard ILU extended by a special care for the main diagonal block associated with the shell structure. In the second approach, the 2×2 structure–fluid system is approximated by the block symmetric Gauss–Seidel preconditioner, where the preconditioner on the fluid part is used as the block solver of the fluid part. In both cases, all fill-ins from the main diagonal block are allowed at the factorization on the structure (I^{∞}), since the submatrices associated with the shell elements are ill-conditioned. In Section 6, efficiencies of the proposed methods are shown and performances of the two preconditioners are compared with numerical experiments for some FEM discretizations of three dimensional fluid–structure interaction problems. The effects of Krylov subspace methods on the present problems in conjunction with the proposed preconditioners and weakly coupled approaches are examined in Section 7.

2. Fluid–structure interaction analysis

This section outlines the fluid–structure interaction analysis method which was developed in [17]. Similar fluid–structure interaction techniques were developed in [1,14]. The ALE method is utilized for deformable fluid domains. We assume the viscous fluid to be isothermal and that $\partial P/\partial\rho = B/\rho$, with B, P and ρ being the fluid bulk modulus, the pressure, and the fluid density, respectively. The ALE form of the Navier–Stokes equations can be expressed as

$$\rho\left.\frac{\partial v_i}{\partial t}\right|_\chi - \rho c_j\frac{\partial v_i}{\partial x_j} = \frac{\partial \sigma_{ji}}{\partial x_j} + \rho g_i \quad \text{in } R_t^{\mathrm{f}}, \tag{1}$$

$$\frac{1}{B}\left.\frac{\partial P}{\partial t}\right|_\chi + \frac{1}{B}c_i\frac{\partial P}{\partial x_i} + \frac{\partial v_i}{\partial x_i} = 0 \quad \text{in } R_t^{\mathrm{f}}, \tag{2}$$

where $\partial(\cdot)/\partial t|_\chi$ is the time derivative in the ALE coordinates χ, the velocity of which is $\mathbf{v}_m$, and the convective velocity $\mathbf{c} = \mathbf{v} - \mathbf{v}_m$. Here σ denotes the Cauchy stresses, $\rho\mathbf{g}$ the body forces, and R_t^{f} denotes the spatial domain of the fluid with the boundary $\partial R_t^{\mathrm{f}}$ at time t. The superscript f stands for the fluid component. The fluid is assumed to be Newtonian. Using the Galerkin method and spatial discretization for Eqs. (1) and (2), we obtain the following equations in the matrix form:

$$M^{\mathrm{V}}\cdot\dot{V} + A^{\mathrm{V}}\cdot V + K_\mu\cdot V - G\cdot P = F^{\mathrm{V}}, \tag{3}$$

$$M^{\mathrm{P}}\cdot\dot{P} + A^{\mathrm{P}}\cdot P + G^{\mathrm{T}}\cdot V = F^{\mathrm{P}}, \tag{4}$$

where M^{V} and M^{P} are the generalized mass matrices for velocity and pressure, respectively, and A^{V} and A^{P} are the generalized matrices of convective terms for velocity and pressure, respectively. Here K_μ is the fluid viscosity matrix, G is the divergence operator matrix, $\dot{P}$ and $\dot{V}$ are the time derivatives of the pressure and velocity vectors, respectively, in ALE coordinates, and F is the external force vector.

Let R_t^{s} be the spatial domain of a structure. Here the superscript s stands for the structural component. The equilibrium equations for structure are:

$$\rho\frac{\mathrm{d}^2u_i}{\mathrm{d}t^2} = \frac{\partial\sigma_{ji}}{\partial x_j} + \rho^{\mathrm{s}}g_i \quad \text{in } R_t^{\mathrm{s}}. \tag{5}$$

Upon total Lagrangian formulation and finite element discretization, a non-linear system of equations is obtained in matrix form, and the incremental form at each time step is given as follows:

$$M^{\mathrm{s}}\Delta\ddot{U} + {}^{t}K^{\mathrm{s}}\Delta U = {}^{t+\Delta t}F - {}^{t}Q^{\mathrm{s}}. \tag{6}$$

Here, M^{s} is the mass matrix, K^{s} the tangent stiffness matrix, and F the external force vector. Q^{s} is composed of the internal and inertial forces of the structure, and $\Delta\ddot{U}$ and ΔU are increments of the acceleration vector and the displacement vector, respectively.

In the strong coupling method the geometrical compatibility and the equilibrium conditions are enforced through the assembly of fluid and structure elements on the interface between the fluid and the structure. For this purpose we define augmented variable vectors as

$$\varphi^{\mathrm{fs}} = \begin{pmatrix} V_i^{\mathrm{f}} \\ P \\ V_{\mathrm{c}} \\ V_i^{\mathrm{s}} \end{pmatrix}, \quad U^{\mathrm{s}} = \begin{pmatrix} - \\ - \\ U_{\mathrm{c}} \\ U_i^{\mathrm{s}} \end{pmatrix}, \tag{7}$$

and thus the system equations are constructed in incremental form as follows:

$$ {}^{t}M^{fs}\Delta\ddot{\varphi}^{fs} + {}^{t}C^{f}\Delta\varphi^{fs} + {}^{t}K^{s}\Delta U^{s} = {}^{t+\Delta t}F - {}^{t}Q^{fs}. \tag{8} $$

Here, V_i^f is the velocity vector of the fluid independent of the structure, P the pressure vector of the fluid, V_c the coupled velocity vector, V_i^s the velocity vector of the structure independent of the fluid, U_c the coupled displacement vector, and U_i^s the displacement vector of the structure independent of the fluid. In Eq. (8), F denotes the external force vector of the coupled system and Q^{fs} the equivalent internal force vector including all effects. M^{fs} denotes the mass matrix composed of those for the fluid and the structure. C^f consists of the divergence, viscous and convective terms of the fluid. K^s is the tangent stiffness matrix of the structure. Note that the ALE conditions are set to be identical to the Lagrangian coordinates on the deformable interface in the strong coupling method.

In the present paper, standard stabilization methods, i.e. SUPG [4] and PSPG methods [16] are used for the fluid analysis. Therefore, Eqs. (3) and (4) are modified as follows:

$$ (M^{V} + M_{\delta})\cdot\dot{V} + (A^{V} + A_{\delta})\cdot V + (K_{\mu} + K_{\mu\delta})\cdot V - (G + G_{\delta})\cdot P = F^{V} + F_{\delta}, \tag{9} $$

$$ M^{P}\cdot\dot{P} + A^{P}\cdot P + G^{T}\cdot V + M_{\epsilon}\cdot\dot{V} + A_{\epsilon}\cdot V + K_{\epsilon}\cdot V + G_{\epsilon}P = F^{P} + F_{\epsilon}. \tag{10} $$

Here, matrices with the subscripts δ and ϵ stem from SUPG and PSPG, respectively. Also, a modified mass matrix [5] is employed for stability in the shell analysis. Including these stabilization terms, the coefficient matrices of Eq. (8) are defined as follows:

$$ M^{fs} = \begin{pmatrix} (M^{V} + M_{\delta})_{ii} & 0 & (M^{V} + M_{\delta})_{ic} & 0 \\ M_{\epsilon i} & M^{P} & M_{\epsilon c} & 0 \\ (M^{V} + M_{\delta})_{ci} & 0 & (M^{V} + M_{\delta} + M^{s}_{mod})_{cc} & (M^{s}_{mod})_{ci} \\ 0 & 0 & (M^{s}_{mod})_{ic} & (M^{s}_{mod})_{ii} \end{pmatrix}, \tag{11} $$

$$ C^{f} = \begin{pmatrix} (A' + A'_{\delta} + K_{\mu} + K_{\mu\delta})_{ii} & -(G + G_{\delta})_{i} & (A' + A'_{\delta} + K_{\mu} + K_{\mu\delta})_{ic} & 0 \\ (G^{T} + A_{\epsilon} + K_{\epsilon})_{i} & A^{P} + G_{\epsilon} & (G^{T} + A_{\epsilon} + K_{\epsilon})_{c} & 0 \\ (A' + A'_{\delta} - K_{\mu} + K_{\mu\delta})_{ci} & -(G + G_{\delta})_{c} & (A' + A'_{\delta} - K_{\mu} + K_{\mu\delta})_{cc} & 0 \\ 0 & 0 & 0 & 0 \end{pmatrix}, \tag{12} $$

$$ K^{s} = \begin{pmatrix} 0 & 0 & 0 & 0 \\ 0 & 0 & 0 & 0 \\ 0 & 0 & K_{cc} & K_{ci} \\ 0 & 0 & K_{ic} & K_{ii} \end{pmatrix}. \tag{13} $$

Here, M^{s}_{mod} denotes the modified mass matrix, and A' the tangent matrix obtained by the linearization of $A\cdot V$. Finally, using the Newmark-β time integration scheme, the following linear system of equations is obtained for the Newton–Raphson iterations.

$$ ({}^{t+\Delta t}M^{fs(k)} + {}^{t+\Delta t}C^{f(k)}\Delta t\gamma + {}^{t+\Delta t}K^{s(k)}\Delta t^{2}\beta)\Delta\ddot{\varphi}^{fs(k)} = {}^{t+\Delta t}R^{(k)}, \tag{14} $$

where ${}^{t+\Delta t}R^{(k)}(= {}^{t+\Delta t}F - {}^{t+\Delta t}Q^{fs(k)})$ is the residual for the kth iteration. γ and β are constants of the Newmark-β method. The ALE mesh motion is controlled after the above computation, i.e., the coordinates of the interior nodes are determined by solving a Laplace equation with the prescribed nodal coordinates on the interface computed from the above equations. The interior nodal velocities are evaluated by just the

time integration algorithm. Then, we return to the above computation. This process is repeated until convergence is reached.

3. Basics of preconditioned Krylov subspace iterative methods and ILU preconditioners

In this section, as background information in introducing the preconditioners we are proposing, we review the general concepts of the preconditioned Krylov subspace methods and non-standard techniques concerning with the ILU factorization. The basics of the ILU factorization will be found in the standard literatures [8].

We start with explaining the convergence behavior of the preconditioned iterative methods by making use of the eigenvalue distribution of the preconditioned system. Let

$$Au = b \tag{15}$$

be the system of linear equations to be solved. If we have an appropriate approximation P of the coefficient matrix A and the solution for the matrix P is easy, the following simple iterative solution scheme can be easily performed.

Setup initial guess u_0;
for $k = 1,\ldots,$
$r_{k-1} = b - Au_{k-1}$; $u_k = u_{k-1} + P^{-1}r_{k-1}$;
next k;

It is easy to see that the following equality holds for the sequence of solutions obtained by the above iteration.

$$Pu_k - (A - P)u_{k-1} = b, \quad k = 0, 1, \ldots. \tag{16}$$

Let $e_k = u - u_k$ be the error for u_k. From Eq. (16), we obtain the following equality for the reduction of the errors.

$$e_k = (P^{-1}A - I)e_{k-1}, \quad k = 0, 1, \ldots. \tag{17}$$

Since the residual r_k is related to the error e_k by $r_k = Ae_k$, we also obtain

$$r_k = (AP^{-1} - I)r_{k-1}, \quad k = 0, 1, \ldots. \tag{18}$$

Let $\{\lambda_i\}$ be the set of all eigenvalues of AP^{-1}. Note that $P^{-1}A$ has the same eigenvalue distribution as AP^{-1}. Eqs. (17) and (18) say that the iteration converges if

$$\rho(AP^{-1} - I) = \max_i |\lambda_i - 1| < 1, \tag{19}$$

and the convergence becomes faster as this spectral radius gets smaller. Unfortunately, it is not easy to construct a matrix P which fulfills this condition for the problem given in (14). Actually, we will see in Section 7 that the convergence may not be achieved even if we have complete solutions for both the fluid and structure parts in P because of the strong interactions between them. Nevertheless, if the eigenvalue distribution of AP^{-1} is localized (the number of extremely small or large eigenvalues is small or they cluster), we are able to achieve fast convergence through the use of preconditioned Krylov subspace methods [8]. We will now show why good convergence can be achieved with the preconditioned Krylov subspace method if the eigenvalue distribution is localized. We start by looking for subspaces which contain the errors and the residuals. By using simple induction, we can prove the fact:

$$u_k \in u_0 + P^{-1}\mathrm{span}(r_0, AP^{-1}r_0, \ldots, (AP^{-1})^{k-1}r_0), \tag{20}$$

$$= u_0 + \mathrm{span}(P^{-1}Ae_0, \ldots, (P^{-1}A)^k e_0). \tag{21}$$

From Eqs. (20) and (21), we obtain the following facts for the errors and the residuals.

$$r_k \in r_0 + \mathrm{span}(AP^{-1}r_0, \ldots, (AP^{-1})^k r_0) = \{\mathscr{P}_k(AP^{-1})r_0 | \mathscr{P}_k(0) = 1\}, \tag{22}$$

$$e_k \in e_0 + \mathrm{span}(P^{-1}Ae_0, \ldots, (P^{-1}A)^k e_0) = \{\mathscr{P}_k(P^{-1}A)e_0 | \mathscr{P}_k(0) = 1\}. \tag{23}$$

Here, $\mathscr{P}_k$ is a polynomial of kth order. Eqs. (22) and (23) show that we can obtain better approximations with either smaller errors or smaller residuals by choosing them from the subspace in Eq. (21). For example, assume that we have only a few extremely large eigenvalues $\lambda_1, \ldots, \lambda_m$ of AP^{-1}, and the other eigenvalues cluster around 1. Then, the following polynomial, which fulfills $\mathscr{P}_k(0) = 1$, may effectively reduce the errors and residuals:

$$\mathscr{P}_k(\lambda) = \left(1 - \frac{\lambda}{\lambda_1}\right) \cdots \left(1 - \frac{\lambda}{\lambda_m}\right)(1 - \lambda)^{k-m}, \quad \text{for } k > m. \tag{24}$$

The components associated with large eigenvalues are annihilated via the first m terms and the components associated with the eigenvalues clustering around 1 are effectively reduced by the last term. This example of polynomials chosen such that $\mathscr{P}_k(0) = 1$ shows that it makes sense to search for solutions in the subspace indicated in Eqs. (20) and (21). There are many ways to obtain the solution in the subspace depending on the targeted measure of the accuracy. In general, such a method for computing appropriate solutions in the subspace is called the preconditioned Krylov subspace method, where the subspaces

$$K_k(AP^{-1}, r_0) = \mathrm{span}(r_0, AP^{-1}r_0, \ldots, (AP^{-1})^{k-1}r_0) \tag{25}$$

are called the Krylov subspaces, and P is called the preconditioner of A. For non-symmetric cases like the present problem, the simplest target may be the squared norm of the residuals:

$$\text{find } u_k \text{ such that } (r_k, r_k) = \min\{(\mathscr{P}_k(AP^{-1})r_0, \mathscr{P}_k(AP^{-1})r_0) | \mathscr{P}_k(0) = 1\}. \tag{26}$$

This optimization problem can be easily solved, for example, by the preconditioned GMRES method [9]. The preconditioned GMRES algorithm is based on the following Arnoldi procedure [8], where the orthonormal basis $\{v_i\}_{i=1,\ldots,m}$ is constructed for the preconditioned matrix AP^{-1}:

$v_1 = r_0 (= b - Au_0)$; $v_1 = v_1/\|v_1\|$
for $i = 1, \ldots, m$;
  $w_i = AP^{-1}v_i$;
  for $j = 1, \ldots, i$;
    $h_{j,i} = (w_i, v_j)$; $w_i = w_i - h_{j,i}v_j$;
  next j;
  $h_{i+1,i} = \|w_i\|$; $v_{i+1} = w_i/h_{i+1,i}$;
next i;

By inspecting the Hessenberg matrix defined by

$$H(m) = (h_{j,i})_{i,j=1,m} = ((AP^{-1}v_j, v_i))_{i,j=1,m}, \quad (h_{j,i} = 0 \text{ for } i + 1 < j), \tag{27}$$

we can see how the matrix AP^{-1} acts on the Krylov subspace. In particular, if $\|Av_m\| \ll 1$, the Krylov subspace $K_m(AP^{-1}, r_0)$ is nearly an invariant subspace of AP^{-1}. Thus, the eigenvalue distribution of $H(m)$ is similar to one of AP^{-1} on $K_m(AP^{-1}, r_0)$. In Section 7, we will examine the Hessenberg matrices to under-

stand why applying weakly coupled approaches or using only our preconditioners leads to divergence, and why the Krylov subspace method is a remedy for this problem.

Next, non-standard fill determination techniques in the ILU factorization applied to our preconditioners are introduced. Let

$$A = (a_{i,j})_{1 \leqslant i,j \leqslant n} \tag{28}$$

be a square matrix to be approximated by the ILU preconditioner. Here, each entry a_{ij} is a small submatrix based on the block structure associated with one variable at a node. An incomplete LU (ILU) preconditioner P for A has the following matrix product form, with strictly lower and upper triangular matrices Q_{L} and Q_{U}, and a diagonal matrix Q_{D}:

$$P = (Q_{\mathrm{D}} + Q_{\mathrm{L}})Q_{\mathrm{D}}^{-1}(Q_{\mathrm{D}} + Q_{\mathrm{U}}). \tag{29}$$

Note that the terms "lower", "upper" and "diagonal" have a block-wise sense along with the block structure of A. The factors Q_{L}, Q_{U} and Q_{D} are uniquely determined for a prescribed index set Ω, which should contain all diagonal entries, by the conditions:

$$P = A \text{ on } \Omega \text{ and } Q_{\mathrm{L}} = 0, \quad Q_{\mathrm{U}} = 0 \text{ on } \Omega^{\mathrm{C}}. \tag{30}$$

Namely, the entries $\{q_{i,j}\}$ in the factors are determined by the equalities:

$$\begin{cases} q_{i,j} = a_{i,j} - \displaystyle\sum_{k<\min(i,j)} q_{i,k}q_{k,k}^{-1}q_{k,j} & \text{if } (i,j) \in \Omega, \\ q_{i,j} = 0 & \text{if } (i,j) \notin \Omega. \end{cases} \tag{31}$$

According to Eq. (31), it is preferable to include an index (i,j) to Ω if one of the terms $q_{i,k}q_{k,k}^{-1}q_{k,j}(k < \min(i,j))$ is large even in the case where $a_{i,j} = 0$. Such an entry in the factors is called a fill-in. In our case, we will determine the fill-ins based on information about the variable which the three nodes i, k and j associate with. We will next explain the algorithm for determining Ω. In that explanation, "vk_i" will imply the variable associated with the node i. Furthermore "$\mathrm{tlev}(\mathrm{vk}_i, \mathrm{vk}_k, \mathrm{vk}_j)$" will imply a prescribed tolerable fill level for cases where a fill-in associated with the variables vk_i and vk_j is generated by the elimination of a node associated with the variable vk_k.

Construction of Ω
$\Omega := \{(i,j)\, a_{i,j} \neq 0\}$;
$\mathrm{lev}_{i,j} := 0$ for $(i,j) \in \Omega$;
for $i = 1, \ldots, n$; **for** $k = 1, \ldots, i-1$ **only for** $(i,k) \in \Omega$;
  for $j = k+1, \ldots, n$ **only for** $(k,j) \in \Omega$;
    if $(\max(\mathrm{lev}_{i,k}, \mathrm{lev}_{k,j}) + 1 \leqslant \mathrm{tlev}(\mathrm{vk}_i, \mathrm{vk}_k, \mathrm{vk}_j)$ and $(i,j) \notin \Omega)$ then
      $\Omega := \Omega \cup (i,j)$; $\mathrm{lev}_{i,j} = \max(\mathrm{lev}_{i,k}, \mathrm{lev}_{k,j}) + 1$;
    end if;
  end j;
end k; **end** i;

In Sections 4.1 and 5.1, appropriate ways for determining the tolerable fill level "tlev" will be given for the fluid-only and fluid–structure interaction problems, respectively. The ILU factorization algorithm with the block structure can also be applied to larger classes of submatrices, for example, submatrices associated with variables if the upper equality in Eq. (31) is relaxed to an approximation. This type of preconditioners will be proposed in Section 4.2 for fluid-only problems and in Section 5.2 for fluid–structure coupling problems.

4. Preconditioners for the velocity–pressure formulations

In this section, we focus on the construction of two preconditioners for the fluid problem. Here, we describe the matrices for the fluid problem in 2×2 form where the first and the second parts correspond to the velocity (V_i^f) and pressure (P) vectors, respectively. We denote the submatrix for the fluid part by

$$A_{ff} = \begin{pmatrix} A_{vv} & A_{vp} \\ A_{pv} & A_{pp} \end{pmatrix}. \tag{32}$$

Here, "v" and "p" stand for the fluid velocity and pressure, respectively. Thus, the first and the second blocks in Eq. (32) correspond to the first and second blocks of the coefficient matrix in Eq. (14), respectively, with the representations given in Eqs. (11)–(13).

4.1. ILU approach

In the first approach, we determine the non-zero pattern Ω_{ff} for the ILU factorization of A_{ff} as follows. Here, the indexes i, k, j correspond to those of Eq. (31), where each index is associated with either three velocity components or a pressure component at a node. Namely, (i,j) is the position where a fill-in is allowed due to the presence of non-zeros (i,k) and (k,j) with $k < \min(i,j)$. Let l be a fill level applied only to the interface parts (1,2) and (2,1) blocks.

(1) No fill-ins are allowed in the (1,1)-block.
(2) Fill-ins up to the level l are allowed in the (1,2)- and (2,1)-blocks.
(3) All fill-ins are allowed for $k \in V_i^f$ and no fill-ins are allowed for $k \in P$ in the (2,2)-block.

The proposed preconditioner is represented by

$$P_{lff} = \begin{pmatrix} E_v + D_v & 0 \\ E_{pv} & E_p + D_p \end{pmatrix} \begin{pmatrix} D_v^{-1} & 0 \\ 0 & D_p^{-1} \end{pmatrix} \begin{pmatrix} D_v + F_v & F_{vp} \\ 0 & D_p + F_p \end{pmatrix}. \tag{33}$$

Here,

$$P_{vv} = (E_v + D_v) D_v^{-1} (D_v + F_v) \tag{34}$$

is the ILU(0) factorization (the number 0 implies that no fill-ins are allowed.) of A_{vv} from the first condition, and $(E_p + D_p) D_p^{-1} (D_p + F_p)$ is the ILU(0) factorization of

$$B_{lpp} = A_{pp} - E_{pv} D_v^{-1} F_{vp}, \tag{35}$$

from the third condition. From Eqs. (11)–(13) $A_{pv} = -A_{vp}^T$ holds in the absence of any stabilization technique. Thus, if A_{vv} and A_{pp} are positive and symmetric and the ILU factorization of A_{vv} is stable, then B_{lpp} is positive and symmetric. Though the stability of their ILU factorizations is, in general, uncertain, they were stable for most cases in our experiments as long as ILU(0) factorization was applied to B_{lpp} and no stabilization techniques are used. Unless a considerably large fill level is chosen, many negative diagonal entries appear if fill-ins are taken into account. Therefore, we strongly recommend the use of ILU(0) factorization for B_{lpp}. As for the velocity part, ILU(0) in Eq. (34) might be a sufficient approximation to A_{vv} because of the presence of the mass matrix part of Eq. (11) in Eq. (14). In [13], a similar ILU factorization is proposed, but without allowing any fill-ins in the (2,2)-block. It was reported that moderate convergence can be realized for finite element discretization with triquadratic Crouzeix–Raviart hexahedrons, using 3×27 velocity unknowns and three pressure unknowns per element. In our case, much simpler FE discretizations (3×8 velocity unknowns and one or eight pressure unknowns per element) are used in order

to keep the computational load small. Instead, we have some difficulty in the treatment of the diagonal block associated with the pressure vector. Thus, having strong preconditioner on the (2, 2)-block is a key issue in our case.

4.2. Incomplete Schur complement approach

In the second approach we start with an approximation:

$$\begin{pmatrix} A_{vv} & A_{vp} \\ A_{pv} & A_{pp} \end{pmatrix} \approx \begin{pmatrix} P_{vv} & A_{vp} \\ A_{pv} & A_{pp} \end{pmatrix}. \tag{36}$$

Here P_{vv} can be any approximation to A_{vv}. In our case we will use the ILU(0) factorization of A_{vv} as represented in Eq. (34). Then an incomplete factorization by variable is applied to the right-hand side of Eq. (36) (instead of the original matrix). The preconditioner can be represented as given in Eq. (37), and can thus be reduced to Eq. (38).

$$P_{2ff} = \begin{pmatrix} P_{vv} & 0 \\ A_{pv} & T_{pp} \end{pmatrix} \begin{pmatrix} P_{vv}^{-1} & 0 \\ 0 & T_{pp}^{-1} \end{pmatrix} \begin{pmatrix} P_{vv} & A_{vp} \\ 0 & T_{pp} \end{pmatrix} \tag{37}$$

$$= \begin{pmatrix} P_{vv} & A_{vp} \\ A_{pv} & T_{pp} + A_{pv} P_{vv}^{-1} A_{vp} \end{pmatrix}. \tag{38}$$

Naturally, the following condition on T_{pp} arises from Eq. (38):

$$T_{pp} \approx S_{pp} = A_{pp} - A_{pv} P_{vv}^{-1} A_{vp}. \tag{39}$$

Here, S_{pp} is the Schur complement for the right-hand side in Eq. (36). Note that there is no need for an explicit representation of T_{pp} and S_{pp} in preconditioning with P_{2ff}. What must be performed in every preconditioning process is just the solution of a linear system with the coefficient matrix T_{pp}. We also note that there is no difficulty in carrying out a matrix-vector multiplication of the form $S_{pp}v$, since it just requires three matrix-vector multiplications with A_{pp}, A_{pv} and A_{vp}, and one preconditioning step with P_{vv}. For these reasons, instead of performing a solution for an explicitly given T_{pp}, we perform a few preconditioned GMRES iterations for the matrix S_{pp} in Eq. (39). As a preconditioner for S_{pp}, we use the ILU(0) factorization of

$$B_{2pp} = A_{pp} - A_{pv} \mathrm{rowsum}(|A_{vv}|)^{-1} A_{vp}, \tag{40}$$

where $|A_{vv}|$ is the matrix whose components are the absolute values of those of A_{vv}, and $\mathrm{rowsum}(|A_{vv}|)$ is the diagonal matrix where all non-diagonal entries are lumped to the diagonal entry in the same row. Benefits arising from taking such a preconditioner for S_{pp} are given in Appendix A. The above preconditioner may give an approximation to S_{pp} on the subspace spanned by its eigenvectors with the smallest eigenvalues. A similar technique is used in [15] to construct a semi-implicit scheme for the Navier–Stokes equations.

Note that the preconditioning matrix is not constant in this approach. Thus, we need to use a Krylov subspace iterative method for the outer iterations that allows varying the preconditioner in every iteration. In our case, FGMRES [10] is adopted.

A disadvantage of this approach is that a solution for S_{pp} is expensive although only a few preconditioned GMRES iterations are performed. On the other hand, an advantage might be robustness in terms of the convergence and stability of the ILU factorization. As shown in Eq. (38), the (1, 2) and (2, 1)-blocks of P_{2ff} and A_{ff} are identical, whereas a lot of fill-ins are needed to fulfill the same condition for the first approach. In addition, better stability is expected for the ILU factorization of Eq. (40) than for B_{1pp} in

Eq. (35), since A_{pv}rowsum $(|A_{vv}|)^{-1}A_{vp}$ in Eq. (40) is more or less a discretized diffusion operator, whereas the symmetry of $E_{pv}D_v^{-1}F_{vp}$ in Eq. (35) may be significantly destroyed when A_{vv} is strongly non-symmetric.

5. Preconditioners for the fluid–structure interaction system

In this section, we extend the preconditioners proposed for the fluid part in Section 4 to the fluid–structure system. Here, we again represent the matrices in 2×2 form, where each of the two parts corresponds to either the fluid vector ($V_i^f \oplus P$) or the structure vector (V^s). The total matrix is defined as

$$A = \begin{pmatrix} A_{ff} & A_{fs} \\ A_{sf} & A_{ss} \end{pmatrix}. \tag{41}$$

In Eq. (41), the first block corresponds to the fluid part. Thus, A_{ff} is identical to the matrix A_{ff} in Eq. (32). The second block corresponds to the third and fourth blocks of the coefficient matrix in Eq. (14), using the representations in Eqs. (11)–(13).

5.1. ILU approach

If the standard ILU factorization with a prescribed non-zero pattern Ω is applied to A_{ff}, there is no difficulty in extending the ILU factorization process to the (1,2), (2,1) and (2,2)-blocks in Eq. (41). Thus, the preconditioner is represented as

$$P_1 := \begin{pmatrix} E_f + D_f & 0 \\ E_{sf} & E_s + D_s \end{pmatrix} \begin{pmatrix} D_f^{-1} & 0 \\ 0 & D_s^{-1} \end{pmatrix} \begin{pmatrix} D_f + F_f & F_{fs} \\ 0 & D_s + F_s \end{pmatrix}. \tag{42}$$

Here, $(E_f + D_f)D_f^{-1}(D_f + F_f)$ is equivalent to the 2×2 form in Eq. (33). For this approach, we use the following fill strategy:

(1) For the (1,1)-block we use the fill strategy described in Section 4.1.
(2) No fill-ins are allowed in the (1,2)- and (2,1)-blocks.
(3) All fill-ins are allowed for $k \in V^s$ and no fill-ins are allowed for $k \in V_i^f \oplus P$ in the (2,2)-block.

As we will see in Section 7, the second condition is sufficient to obtain a reasonable approximation to the interaction part for the present problem. The third condition is due to the ill-conditioned property of matrices resulting from the use of shell elements.

5.2. Symmetric Gauss–Seidel approach

If we put the fluid part into the first block of the 2×2 fluid–structure system and obtain its approximate block LU factorization, then we have to solve the linear system on the fluid part twice (once for each of the forward and backward substitutions). This is not a good idea since the preconditioner in the second approach for the fluid part is expensive. To avoid this, we put the fluid part into the second part and extend the second approach by approximating the total system by a block symmetric Gauss–Seidel preconditioner, defined as

$$P_2 := \begin{pmatrix} A_{ss} & 0 \\ A_{fs} & P_{2ff} \end{pmatrix} \begin{pmatrix} A_{ss}^{-1} & 0 \\ 0 & P_{2ff}^{-1} \end{pmatrix} \begin{pmatrix} A_{ss} & A_{sf} \\ 0 & P_{2ff} \end{pmatrix}. \tag{43}$$

Here, the linear system for A_{ss} is solved via a standard forward and backward substitutions with the sparse LU factors. This approach provides poorer approximation to the interaction part than the approach in Section 5.1. However, we will see that this difficulty is overcome by the use of Krylov subspace methods, since the dimensions of the problematic modes in the interaction part are small for the problems considered.

6. Comparisons of the two preconditioners

In this section, numerical experiments are performed for some FEM discretizations. The element types tested here in the fluid domain are the $Q1/P0$ and $Q1/Q1$ elements on a hexahedron. In the $Q1/P0$ element, the velocities are interpolated with trilinear functions and the pressure is interpolated with a constant. In the $Q1/Q1$ element, both the velocities and the pressure are interpolated with trilinear functions.

As for the relationship with the stabilization techniques, the following observations are made from Eqs. (11)–(13) in terms of the matrix structures.

- When the SUPG formulation is used, A_{vv} is different from the one without the SUPG formulation. In case of $Q1/Q1$, A_{vp} is also different. In Eq. (9), the term A_δ brings a certain stabilization effect. However, the term M_δ reinforces the non-diagonal entries, and the term G_δ breaks the symmetry for the interaction between the pressure and the velocity. The latter changes may create negative effects for the convergence of the iterative methods.
- When the PSPG formulation is used, A_{pv} and A_{pp} are different from the ones without the PSPG formulation. In Eq. (10), the term G_ϵ brings an essential stabilization effect. However, the terms M_ϵ and A_ϵ break the symmetry for the interaction between the pressure and the velocity. The latter changes may create negative effects for the convergence of the iterative methods.

One of the important facts to be recognized is that $A_{pv} = -A_{vp}^{T}$ does not hold anymore in case of $Q1/Q1$ when either SUPG or PSPG stabilization is used. This might be disadvantageous to the stability of the ILU factorization of B_{1pp} in Eq. (35) and B_{2pp} in Eq. (40).

The test problem is a fluid–structure coupling analysis of a cylinder (length $L = 0.2$ m, diameter $D = 0.1$ m). Here, we assume that one end of the cylinder is covered with a deformable diaphragm, which is modeled by MITC shell elements [3]. A uniform velocity distribution in the axial direction is applied to the other end assuming the following time history:

$$v(t) = \frac{\pi L}{NT} \sin\left(\frac{2\pi t}{T}\right) \text{ m/s}, \quad 0.0 \leqslant t \leqslant T = 1.0 \text{ s}, \ N = 20. \tag{44}$$

On the wall of the cylinder and the diaphragm, non-slip conditions are prescribed. The amount of water that crosses the inflow boundary reaches its peak value at $t = 0.5$ s, and that maximum amount is approximately 1/20 of the cylinder volume. No boundary condition is specified for the pressure. The material properties for the fluid are as follows: mass density $\rho = 9.982 \times 10^2 \text{ kg/m}^3$, viscosity $\mu = 1.002 \times 10^{-3}$ Pa, bulk modulus $B = 2.2 \times 10^9$ Pa. The material properties for the diaphragm are: Young's modulus $E = 2.0 \times 10^7$ Pa, Poisson's ratio $\nu = 0.45$, mass density $\rho = 1.13 \times 10^3 \text{ kg/m}^3$, and the thickness $t = 0.20$ mm.

Here, we examine the performance using the three types of meshes shown in Fig. 1. Except for the thin elements at the boundary layers, the ratios of mesh sizes are approximately 1:2/3:1/2. Detailed information on the number of unknowns and the number of non-zero entries in the corresponding matrices are given in Table 1. Such a test is useful for estimating the growth of the number of iterations in relation to the sizes of the meshes used.

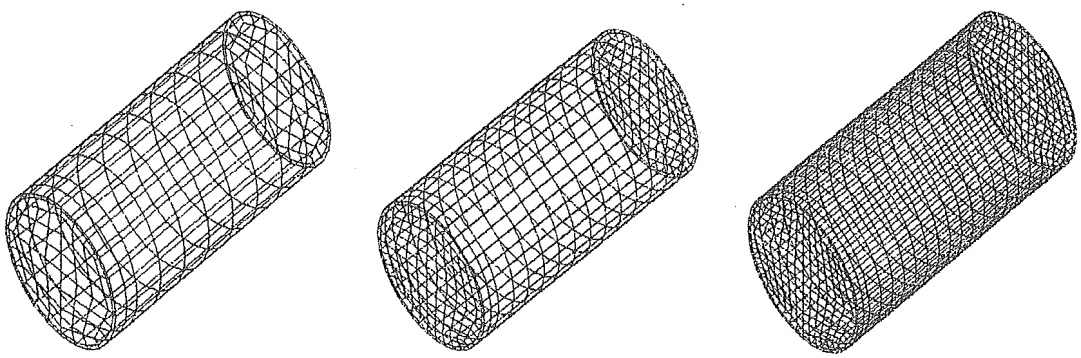

Fig. 1. Meshes with three different levels of refinement.

Table 1
The mesh and matrix sizes for the test problem

Mesh	V_1^f	P	V^*	Total	nz(A)
Q1/P0C	1971	840	413	3224	190036
Q1/P0M	5712	2295	752	8759	545371
Q1/P0F	12369	4800	1181	18350	1179370
Q1/Q1C	1971	1067	413	3451	293873
Q1/Q1M	5712	2752	752	9216	835012
Q1/Q1F	12369	5565	1181	19115	1797137

In the columns of V_1^f, P and V^*, the number of unknowns of these vector spaces are noted. nz(A) is the number of non-zeros of the coefficient matrix A. In the first column, C, M and F mean coarse, medium and fine, respectively.

In the present performance test, the matrix given at $t = 0.5$ s is used. At this time, the deformation of the diaphragm reaches its peak since the volume of the fluid inside the cylinder is at its maximum. Fig. 2 shows the velocity distribution and the diaphragm deformation for the mesh *Q1/Q1F*.

In the first ILU based approach, the preconditioners are denoted by ILU-VP(l) where l is the fill level applied to the fluid velocity–pressure coupling part.

In the second approach, the inner GMRES iterations for computing the pressure variables are performed until the number of iterations reaches a prescribed number m_{in} or the relative L2-norm of the residual becomes less than 0.1. Here, we examine the cases with $m_{in} = 5$ and $m_{in} = 10$. For the present boundary conditions (no boundary values for the pressure), the row sum of A_{vp} is zero for all the rows. Thus, the operator $-A_{pv}P_{vv}^{-1}A_{vp}$ has a one dimensional null space composed of constant vectors. On the other hand, without the PSPG technique, A_{pp} has almost negligible positive diagonal entries (due to the time derivative in Eq. (2)) compared to the non-zeros in $-A_{pv}P_{vv}^{-1}A_{vp}$. Thus, we may have one extremely small eigenvalue for S_{pp}. This may cause difficulty in the convergence of the inner GMRES iterations. To prevent this we construct an optimal initial guess within the constant pressure vector space before entering the inner GMRES iterations. The details of this optimization procedure are given in Appendix B. This optimization process is economical in terms of computation time and harmless even if pressure boundary values are given. We also apply a simple remedy, in the case where the ILU factorization of B_{2pp} breaks down, which consists of just adding an appropriate positive constant to the diagonal of B_{2pp}. As a first try we start by adding $0.001 \times \alpha$, where α is the average of the diagonal entries of B_{2pp}. If that fails, we add $0.01 \times \alpha$ and so on. Note that we

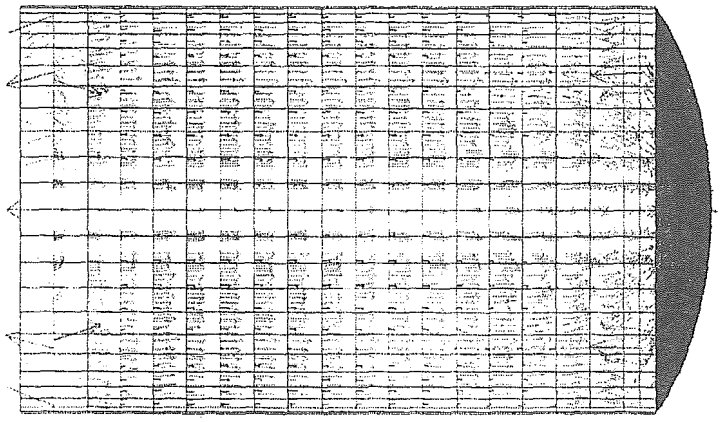

Fig. 2. Velocity field and diaphragm deformation at (the peak) $t = 0.5$s for mesh $Q1/Q1F$.

count this additional computation time in the setup time for our timing measurements. It turns out that the factorization cost for B_{2pp} is very low compared to the iterative solution process. Thus, a few tries are not problematic. Such tries of ILU factorization never occur for $Q1/Q1$ with the pressure stabilization technique, although a few negative diagonal components were found in some $Q1/P0$ cases. Although it is basically possible to apply a similar technique to the ILU factorization on the pressure part in the first approach, we do not apply it to the present numerical experiments. The ILU factorization in the first approach is implemented in the same way as the standard block ILU factorization with a specified non-zero block set Ω.

In the following, we present the results using the $Q1/P0$ element with and without SUPG stabilization, while for the $Q1/Q1$ element we present the results with SUPG and PSPG stabilizations. In the timing results, the CPU time consumed for setting up the preconditioner is also listed. The tests were performed on a Linux PC with Intel(R) Pentium(R) IV processor (2GHz, 512Kb cache). The GMRES and the outer FGMRES iterations were restarted every 200 iterations for all cases. The iterative process was terminated when the relative L2-norm of the residual became less than 10^{-12}.

First, we examine the results obtained for $Q1/P0$ without any stabilization in Table 2. Here, the second approach is denoted by SGS-Schur. We see that ILU-VP(0) provides a very slow convergence even though the ILU factorizations are accomplished without any singularity. However, the convergence is considerably improved by using ILU-VP(1). Note that the number of non-zeros for ILU-VP(1) is twice the number for ILU-VP(0). Thus, the computational load for the ILU-VP(1) factorization is nearly eight times as high as for the ILU-VP(0). Hence, the setup takes a considerable amount of time compared to the total CPU time. The number of iterations with ILU-VP(1) increases almost proportionally to the number of nodes in the meshes in each direction, i.e. the inverse of the mesh size h^{-1}. This is known as typical behavior of the ILU preconditioned methods applied to second-order elliptic problems. On the other hand, the number of iterations with SGS-Schur seems almost independent of the number of nodes in the meshes. Thus, the growth of the CPU time is almost proportional to the number of unknowns as shown in Table 2. Since there are no fill-ins in the fluid velocity–pressure coupling part, the non-zero pattern of B_{2pp} is the same as for B_{1pp}. Thus, the setup time for SGS-Schur is as small as that for ILU-VP(0). For these reasons, it can be said that the larger the mesh size, the clearer the superiority of SGS-Schur over ILU-VP(1). Note that most of the inner GMRES iterations are terminated at the 10th iteration in this test case. Since the inf-sup condition is not satisfied and the stabilization technique is not applicable to the pressure part for this element, the SGS-Schur approach sometimes shows strange behavior. For example, in the result for

Table 2
Comparison of the performance for $Q1/P0$ without any stabilization technique

Mesh	nz(ILU)	ɀneg	ɀitr.	S-time	I-time	T-time
ILU-VP(0)						
C	278766	0	387	0.08	2.85	2.93
M	788937	0	752	0.26	15.43	15.69
F	1690930	0	952	0.63	44.81	45.44
ILU-VP(1)						
C	491594	0	67	0.54	0.74	1.28
M	1456137	0	87	1.61	2.75	4.36
F	3194066	0	109	4.18	8.10	12.28

Mesh	ɀouter	ɀinner	S-time	I-time	T-time
SGS-Schur ($m_{in} = 5$)					
C	59	295	0.06	1.33	1.39
M	54	270	0.22	3.74	3.96
F	44	220	0.52	6.59	7.11
SGS-Schur ($m_{in} = 10$)					
C	29	288	0.05	1.06	1.11
M	42	417	0.22	4.34	4.56
F	28	277	0.52	6.24	6.76

nz(ILU) is the number of non-zero entries of the ILU factors. ɀneg is the number of negative diagonal entries found in the ILU factors. ɀitr. is number of iterations to reach convergence. S-time, I-time and T-time are the times in seconds for the setup, the iterative process and the total execution, respectively. In SGS-Schur, ɀouter is the number of outer FGMRES iterations, and ɀinner is the sum of the inner GMRES iterations.

$m_{in} = 10$, the number of iterations for the medium size mesh is remarkably larger than the other two meshes.

The next test case is $Q1/P0$ with SUPG stabilization. From Table 3, it seems as if this stabilization shows negative effects on the convergence of the iterative method. Column "ɀneg" shows the instability of the factorizations at the pressure part whenever we use ILU-VP. However, the third and fourth tables show that such instabilities are eliminated by applying the factorization to the matrix without SUPG terms. Although we lower the level of the approximation to some extent with this trick, it seems more important to maintain factorization stability. In the case of $Q1/P0$, the relationship $A_{pv} = -A_{vp}^{T}$ from Eq. (32) still holds for using SUPG stabilization. However, the antisymmetry of A_{vv} tends to increase with stabilization, and this, in turn, seems to increase the difference between E_{pv} and $-F_{vp}^{T}$ in Eq. (35). When we use SGS-Schur, we can also see that the use of the stabilization causes an increase of the number of outer iterations. However, SGS-Schur seems superior to ILU-VP with and without the use of SUPG stabilization for problems with large mesh size.

Finally, we examine the results for $Q1/Q1$ with SUPG and PSPG stabilizations in Table 4. As stated earlier, the stabilization techniques substantially alter A_{pv} and A_{vp} from the original discretization. We observe that even some negative diagonal entries appear in $-A_{pv}\mathrm{rowsum}(|A_{vv}|)^{-1}A_{vp}$. However, this is overcome by PSPG stabilization to A_{pp}. In fact, with this stabilized A_{pp}, the ILU factorization of B_{2pp} can always be successfully completed without adding positive values, and better convergence for S_{pp} is achieved than with the use of $Q1/P0$ elements. As for ILU-VP(1), a remarkably large amount of CPU time is consumed by the factorization. This behavior can be explained as follows: A fill-in in the fluid velocity–pressure block connects the pressure variable to the velocity variable on a node, that is not a direct neighbor, but neighbors a direct neighbor. Thus, the elimination of a velocity node connects two pressure variables within the set of 4th neighboring nodes. Thus, B_{1pp} in Eq. (35) becomes a very dense matrix in this case. It is obvious that the